JOURNAL OF COMPUTATIONAL PHYSICS 100, 424–429 (1992)

NOTE

A Numerical Method for Systems of Conservation Laws of Mixed Type Admitting Hyperbolic Flux Splitting*

1. INTRODUCTION

The system of conservation laws

$$\begin{aligned} \mathbf{u}_t + \mathbf{f}(\mathbf{u})_x &= 0 \\ \mathbf{u}(x, 0) &= \mathbf{u}^0(x) \end{aligned} \tag{1.1}$$

is hyperbolic if the Jacobian $\partial \mathbf{f}(\mathbf{u})/\partial \mathbf{u}$ has real eigenvalues and a complete set of eigenvectors. Among recent activity in designing stable and accurate numerical methods for solving systems of hyperbolic conservation laws, the ENO (essentially non-oscillatory) high order finite difference method, [6, 7, 16, 17], is quite successful. The philosophy of ENO schemes is to use upwinding and adaptive stencils, based on the local "wind" direction (the sign of the relevant eigenvalue) and the local smoothness, in each of the local characteristic fields. ENO schemes produce sharp, non-oscillatory shock transitions and uniform high order in smooth regions, suitable for solving problems with both shocks and rich smooth region structures.

If the Jacobian $\partial \mathbf{f}(\mathbf{u})/\partial \mathbf{u}$ in (1.1) has complex eigenvalues, the system becomes elliptic. Examples of mixed hyperbolic–elliptic systems include equations in fluid dynamics [20], elasticity [9], and the partial differential equations related to Lorenz systems [8], just to name a few. The solution often involves shocks across the elliptic region, also known as "phase transitions." Since there can be more than one weak solution, some admissibility criteria are needed, with the goal to single out "physically relevant" weak solutions, see, e.g., [11, 12, 3, 18, 19, 9, 4, 14, 15, 10]. The analysis usually starts with the Riemann problem,

$$\mathbf{u}(x, 0) = \begin{cases} \mathbf{u}_L, & x < 0 \\ \mathbf{u}_R, & x > 0. \end{cases} \tag{1.2}$$

More general initial data is more difficult to analyse theoretically. An efficient computational method may be used as a tool to analyse the solutions (e.g., [1]). From a computational point of view, if a shock capturing method, such as the ENO method in [7, 17] is to be used, discontinuities are typically spread out in two or three points; hence points can sit in elliptic regions even if the exact solution jumps across it, making it necessary to treat elliptic regions carefully in order to avoid numerical instability.

Previous numerical calculations for mixed type systems using first-order monotone schemes can be found in, e.g., [1, 10]. For a review of numerical methods in applications see [21]. Successful hyperbolic techniques (upwinding in the hyperbolic regions, artificial viscosity) are used in these references. One of the main ingredients of hyperbolic ENO schemes, and of many other non-oscillatory hyperbolic schemes such as TVD (total-variation-diminishing) schemes [5], is the approximation in each of the local characteristic fields. If the system becomes elliptic, local characteristic decomposition is no longer available. In this paper we treat elliptic regions using hyperbolic flux-splitting and high order methods. In Section 2 we propose a flux splitting $\mathbf{f}(\mathbf{u}) = \mathbf{f}^+(\mathbf{u}) + \mathbf{f}^-(\mathbf{u})$, with the corresponding Jacobians $\partial \mathbf{f}^{\pm}(\mathbf{u})/\partial \mathbf{u}$ having real and positive/negative eigenvalues. This is similar to the flux splitting used for hyperbolic systems, for example, the Lax–Friedrichs splitting and the van Leer splitting [23], but our generalization to elliptic regions of such splitting allows us to handle mixed type systems in a unified and heuristically stable (see Remark 2.2) fashion. The hyperbolic ENO operator is applied separately on $\mathbf{f}^+(\mathbf{u})_x$ and on $\mathbf{f}^-(\mathbf{u})_x$. In this paper we use the van der Waals equation in fluid dynamics

$$\begin{aligned} v_t + p(w)_x &= 0, & w_t - v_x &= 0, \\ v(x, 0) &= v^0(x), & w(x, 0) &= w^0(x), \end{aligned} \tag{1.3}$$

with

$$p(w) = \frac{RT}{w - b} - \frac{a}{w^2}, \tag{1.4}$$

where R, T, a, b are all positive constants, for our numerical examples. See, for example, [20] for details. Equation (1.3)

* Research supported by NSF Grant DMS-88-10150, NASA Langley Grant NAG-1-1145, AFOSR Grant 90-0093, and by NASA Contract NAS1-18605 while the author was in residence at ICASE, NASA Langley Research Center, Hampton, VA 23665.

0021-9991/92 $5.00

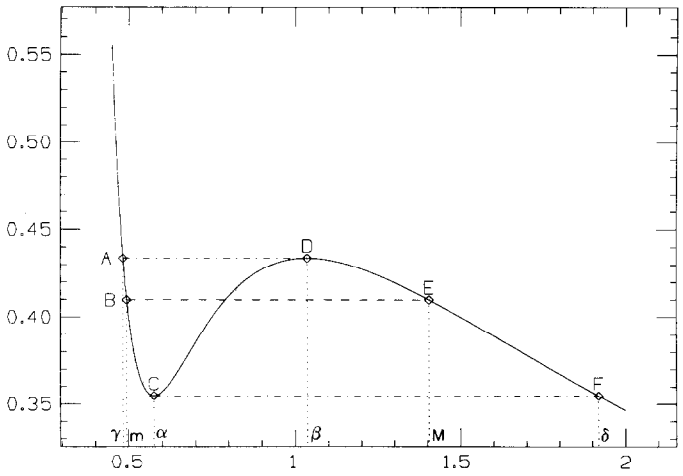

FIG. 1. $p(w) = 1/(w-0.25) - 0.9/w^2$.

corresponds to (1.1) with $\mathbf{u} = (v, w)^T$, $\mathbf{f}(\mathbf{u}) = (p(w), -v)^T$. The two eigenvalues of the Jacobian $\partial \mathbf{f}(\mathbf{u})/\partial \mathbf{u}$ are $\pm\sqrt{-p'(w)}$. For an ideal gas, the pressure $p(w)$ is a decreasing function of w, resulting in a hyperbolic system (1.3). However, during a gas–liquid phase transition, $p'(w)$ may become positive within an interval, as in the case (1.4) with suitable parameters (Fig. 1), making the system (1.3) elliptic in this region. In Section 3 we numerically test our scheme on (1.3). We observe convergence with good resolution to weak solutions for various Riemann problems. These weak solutions are then numerically checked to be admissible under the viscosity–capillarity criterion [18]. We also compute the solution with smooth periodic initial conditions and observe the interesting phenomena of the shrinking of elliptic regions if they are present in the initial conditions.

2. THE NUMERICAL SCHEME

We start with the effort to find a hyperbolic flux splitting

$$\mathbf{f}(\mathbf{u}) = \mathbf{f}^+(\mathbf{u}) + \mathbf{f}^-(\mathbf{u}). \tag{2.1}$$

The requirement is that the Jacobian $\partial \mathbf{f}^+(\mathbf{u})/\partial \mathbf{u}$ has only real and positive eigenvalues, and likewise that the Jacobian $\partial \mathbf{f}^-(\mathbf{u})/\partial \mathbf{u}$ has only real and negative eigenvalues. If the system is hyperbolic, the simplest way to achieve such a splitting is due to Lax–Friedrichs,

$$\mathbf{f}^\pm(\mathbf{u}) = \tfrac{1}{2}(\mathbf{f}(\mathbf{u}) \pm \alpha \mathbf{u}), \qquad \alpha = \max_{i,\mathbf{u}} |\lambda_i(\mathbf{u})|, \tag{2.2}$$

where $\lambda_i(\mathbf{u})$ are the eigenvalues of the Jacobian $\partial \mathbf{f}(\mathbf{u})/\partial \mathbf{u}$. For special classes of hyperbolic systems, such as the Euler equations of a polytropic gas, more sophiscated splittings with better physical meanings are available, e.g., van Leer's splitting [23]. For an elliptic system, the simple splitting (2.2) no longer works. In fact, any splitting with the Jacobians $\partial \mathbf{f}^+(\mathbf{u})/\partial \mathbf{u}$ and $\partial \mathbf{f}^-(\mathbf{u})/\partial \mathbf{u}$ commuting with each other, as is the case in (2.2), will probably fail, because commuting matrices with distinct eigenvalues can be simultaneously diagonalized; hence the eigenvalues of their sum are simply the sum of their corresponding eigenvalues. However, a splitting similar to (2.2) with the scalar α replaced by a diagonal matrix:

$$\mathbf{f}^\pm(\mathbf{u} = \frac{1}{2}(\mathbf{f}(\mathbf{u}) \pm \bar{\alpha}\mathbf{u}), \qquad \bar{\alpha} = \begin{pmatrix} \alpha_1 & & & \\ & \alpha_2 & & \\ & & \ddots & \\ & & & \alpha_m \end{pmatrix} \tag{2.3}$$

can usually yield the required result. For example, the flux $\mathbf{f}(\mathbf{u})$ in the van der Waals equation (1.3) can be split successfully using (2.3) with

$$\alpha_2 = \max_w \left(\max \left(0, \frac{\sqrt{M^2 - 4p'(w)} - M}{2} \right) \right), \qquad \alpha_1 = \alpha_2 + M \tag{2.4}$$

and

$$M = a \max_w \sqrt{\max(0, p'(w))}, \qquad a > 2. \tag{2.5}$$

The idea is to make an ansatz $\mathbf{g}(\mathbf{u}) = M(v, 0)^T$, then try to find the smallest possible M such that the Jacobians $\partial(\mathbf{f}(\mathbf{u}) \pm \mathbf{g}(\mathbf{u}))/\partial \mathbf{u}$ both have real and distinct eigenvalues. This leads to M given by (2.5). Once this is done, it is easy to use the Lax–Friedrichs idea, i.e., to add and substract $\alpha \mathbf{u}$ with a suitable α, to accomplish the splitting. Similar splitting exists for the PDE related to the Lorenz system [5]. In fact, it is easy to prove that this approach works for all 2×2 and at least some higher order systems.

Equipped with the splitting (2.1), one can then apply any successful hyperbolic approximation techniques separately to $\mathbf{f}^+(\mathbf{u})$ and $\mathbf{f}^-(\mathbf{u})$. The only exception is that characteristic decompositions should not be performed in elliptic regions, since the characteristic directions of $\partial \mathbf{f}^+(\mathbf{u})/\partial \mathbf{u}$ and $\partial \mathbf{f}^-(\mathbf{u})/\partial \mathbf{u}$ do not have any physical meaning. In this paper we apply the third order in space and time (fourth order in smooth monotone regions) ENO techniques developed in [16, 17] to $\mathbf{f}^+(\mathbf{u})$ and $\mathbf{f}^-(\mathbf{u})$. See [16, 17] for details.

Remark 2.1. Since the schemes we use are conservative, any converged solution will be a weak solution of (1.1). It is more difficult to show that the limit solutions satisfy various admissibility conditions. If we take the first-order ENO and use the splitting (2.1)–(2.2) for a *hyperbolic* system, we recover the classical Lax–Friedrichs scheme. It is well known that the Lax–Friedrichs scheme can be rewritten as

a centered scheme plus a dissipation term approximately equal to $\frac{1}{2}\alpha\,\Delta x\,\mathbf{u}_{xx}$. If we still take the first-order ENO but use the splitting of the form (2.3) for a mixed type system, we obtain a centered scheme plus a dissipation term approximately equal to $\frac{1}{2}\bar{\alpha}\,\Delta x\,\mathbf{u}_{xx}$, where $\bar{\alpha}$ is the positive diagonal matrix (2.3). It is then reasonable, cf. [11, 19], to expect that the scheme converges to weak solutions satisfying viscosity type admissibility conditions. Ample numerical tests should be performed to assess the convergence and admissability for higher order schemes. The numerical examples in Section 3 are preliminary results in this direction.

Remark 2.2. If some fractional step method (e.g., Strang [22]) is used on the splitting (2.1), we end up with a scheme of the form

$$\mathbf{u}^{n+1} = (\mathbf{I} + \Delta t\,\mathbf{L}^{+})(\mathbf{I} + \Delta t\,\mathbf{L}^{-})\,\mathbf{u}^{n}, \tag{2.6}$$

where $\mathbf{L}^{\pm}$ are hyperbolic operators approximating $\mathbf{f}^{\pm}(\mathbf{u})_x$ (for the next time step the two operators may reverse order). It is easy to choose stable operators $(\mathbf{I} + \Delta t\,\mathbf{L}^{\pm})$, due to the hyperbolicity of $\mathbf{f}^{\pm}(\mathbf{u})$ in (2.1). However, this does not necessarily mean that the scheme (2.6) is stable, since $(\mathbf{I} + \Delta t\,\mathbf{L}^{\pm})$ may not commute with each other and may not be simultaneously diagonalizable. If the operators satisfy the more restrictive condition

$$\begin{aligned} &\|\mathbf{I} + \Delta t\,\mathbf{L}^{+}\| \leqslant 1 + O(\Delta t), \\ &\|\mathbf{I} + \Delta t\,\mathbf{L}^{-}\| \leqslant 1 + O(\Delta t) \end{aligned} \tag{2.7}$$

for any consistent norm, the fractional step scheme (2.6) will be stable.

3. NUMERICAL EXAMPLES

We use the van der Waals equation (1.3)–(1.4) with $RT = 1$, $a = 0.9$, and $b = 0.25$. The graph of the corresponding $p(w)$ is in Fig. 1. The system is elliptic for $\alpha < w \leqslant \beta$, where $\alpha = 0.574912$ and $\beta = 1.036251$. The so-called Maxwell line BF in Fig. 1, where the two shaded areas are equal, intersects the curve of $p(w)$ at $w = m = 0.494273$ and $w = M = 1.405065$. The horizontal lines AD and CF in Fig. 1 yield $\gamma = 0.483100$ and $\delta = 1.918618$.

We use the third-order ENO scheme which is fourth order in smooth monotone regions. If the computational cell is contained completely inside one of the hyperbolic regions $w \leqslant \alpha$ or $w \geqslant \beta$, we use characteristic decompositions (the ENO-LF algorithm described in [16, 17]). Otherwise a component by component ENO approximation is used for computing the numerical flux. The splitting used is (2.3)–(2.5) with $a = 2.2$. The time step Δt is restricted by a CFL number 0.6; i.e., $\Delta t \leqslant 0.6(\rho(\partial \mathbf{f}^{+}(\mathbf{u})/\partial \mathbf{u}) + \rho(\partial \mathbf{f}^{-}(\mathbf{u})/\partial \mathbf{u}))\,\Delta x$, where $\rho(A)$ is the spectral radius of A.

All the computations are performed by using a sequence of refined meshes to verify convergence, although we typically only show the graphs for one or two fixed meshes. Different splittings obtained by varying a in (2.5) or by making another ansatz $\mathbf{g}(\mathbf{u}) = M(0, v)^T$ (see the line after (2.5)) are also tested. We observe no significant difference for third-order ENO although the first-order scheme shows more sensitivity to different splitting, such as different smearing. This is consistent with our experience in hyperbolic calculations, that the difference due to different building blocks (splitting) diminishes as the order of the scheme increases, provided that the building blocks have adequate viscosity. We have also made comparisons between first-order and third-order schemes. They converge to the same solution but the first-order scheme takes at least three to four times more points to get the same resolution of shocks as the third-order ENO does. This would be more apparent if the solution contained some structure in smooth regions. We omit the graphs for these comparisons.

We first compute several Riemann problems (1.2). Boundary points are in the hyperbolic regions and the usual characteristic boundary conditions are used:

(1) $(v_L, w_L) = (1, m)$, $(v_R, w_R) = (1, M)$, where m and M are the Maxwell values defined above. This initial condition satisfies the Rankine–Hugoniot condition for a stationary jump. Physical principles (Maxwell equal area rule) and many admissibility criteria (e.g., the viscosity–capillarity criterion in [18]) indicate that this is an admissible jump. Our numerical result shows a stable, sharp jump for this case, Fig. 2. We remark that here and in what follows, the numerical solution usually has one or two transition points in the elliptic region for the phase jump.

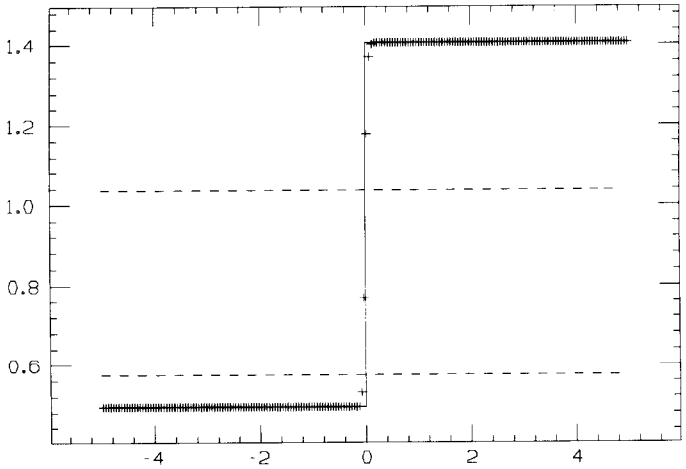

FIG. 2. Maxwell solution, $(v_L, w_L) = (1, m)$, $(v_R, w_R) = (1, M)$, $t = 25$. Two hundred points (+) and the exact solution (solid line). Here and in what follows, the region between the two dashed lines is elliptic.

Apparently they have not caused any instability to the computation.

(2) $(v_L, w_L) = (1, 0.54)$, $(v_R, w_R) = (1, 1.8517)$. This initial condition also satisfies the Rankine–Hugoniot condition for a stationary jump, but physical principles and many admissibility criteria (e.g., the viscosity–capillarity criterion in [18], see also [14]) indicate that this is *not* an admissible jump. Our numerical result shows the evolution of this jump into a more complicated structure of jumps, Fig. 3a, apparently due to the inherent numerical viscosity of the scheme (see Remark 2.1). The solution exhibits oscillatory behaviors near the phase boundary, Fig. 3a. This is unpleasant but not surprising, since we used component by component approximations in cells involving elliptic regions; hence during the process of one wave splitting into two or more waves, one or more of them being hyperbolic, oscillations occur as a failure of recognition of the corresponding characteristic fields. Similar oscillations also appear for hyperbolic systems if a component by component approximation is used (see, e.g., [2]). The oscillations become smaller (hence they are not Gibbs oscillations) and more confined when the number of grids is increased (Fig. 3b), indicating the convergence of the scheme. Also, these oscillations are more apparent for slow moving shocks (see [13]), if we compare Fig. 3a and 4a.

The solid line in Fig. 3a is computed by the same scheme with 2000 points. It agrees with the result with 4000 points; hence it can be considered as a converged solution. In order to check whether this weak solution is admissible under the viscosity–capillarity criterion [18], i.e., whether it is the bounded a.e. limit of $\mathbf{u}^\varepsilon = (v^\varepsilon, w^\varepsilon)$, satisfying

$$\begin{aligned} &v_t^\varepsilon + p(w^\varepsilon)_x = \varepsilon v_{xx} - \varepsilon^2 A w_{xxx}, \\ &w_t^\varepsilon - v_x^\varepsilon = 0 \\ &v^\varepsilon(x, 0) = v^0(x), \qquad w^\varepsilon(x, 0) = w^0(x) \end{aligned} \tag{3.1}$$

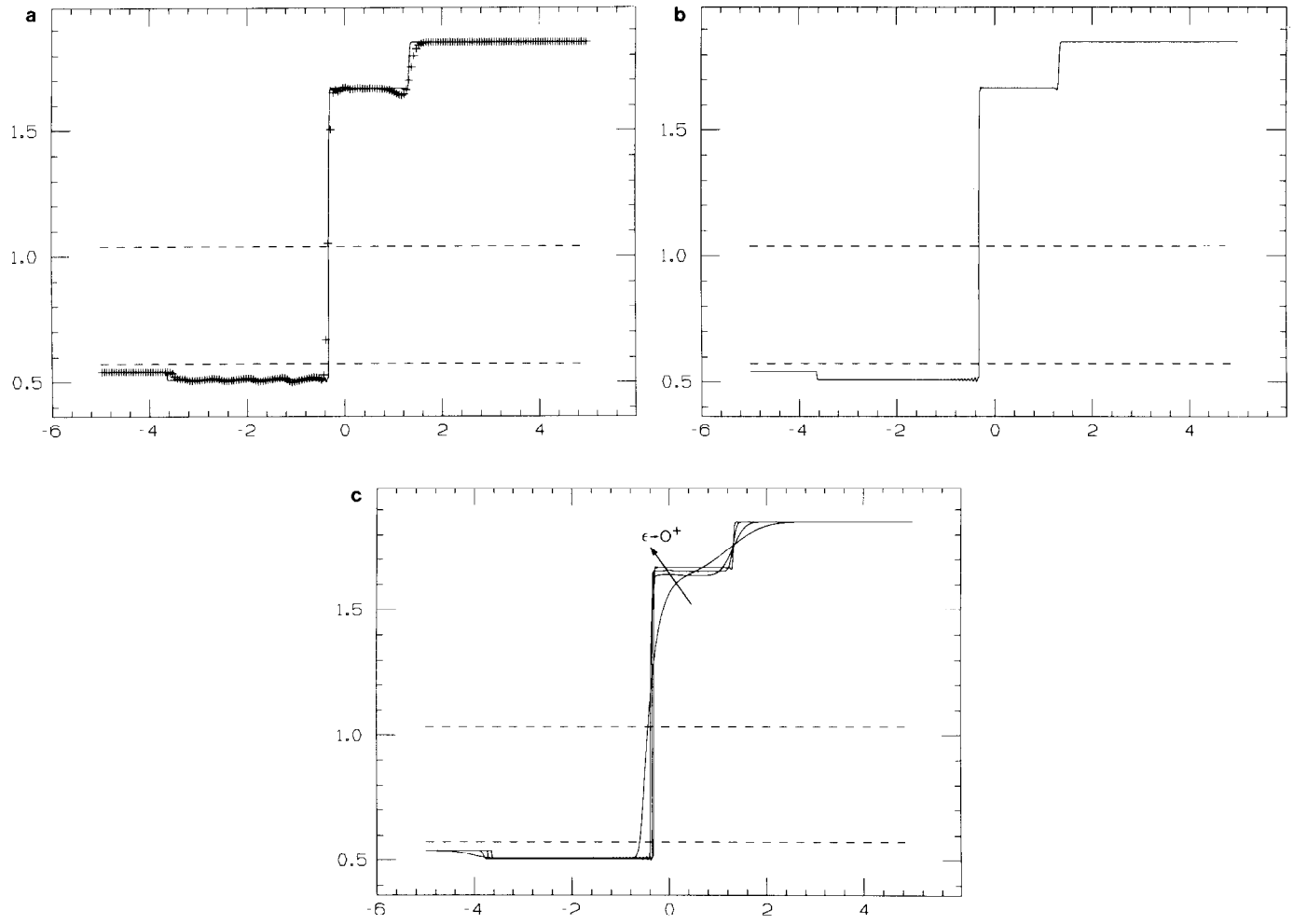

FIG. 3. $(v_L, w_L) = (1, 0.54)$, $(v_R, W_R) = (1, 1.8517)$, $t = 4$. (a) 200 points (+) and 2000 points (solid line); (b) 2000 points; (c) centered solutions of (3.1) with $\varepsilon = 0.1, 0.01, 0.001$, and ENO solution for (1.3).

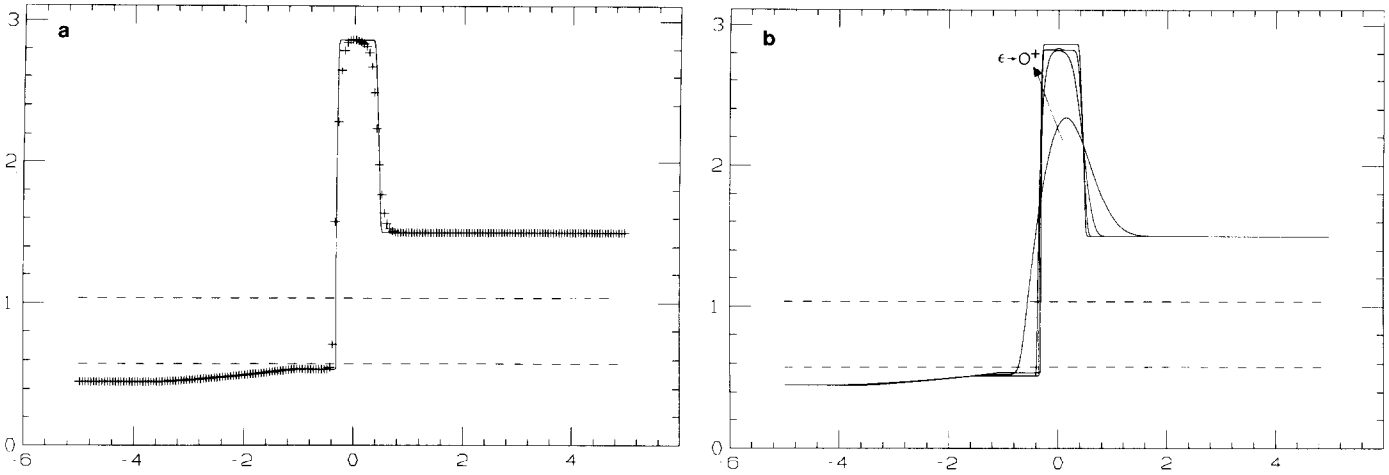

FIG. 4. $(v_L, w_L) = (1, 0.45)$, $(v_R, w_R) = (2, 1.5)$, $t = 1.5$. (a) 200 points (+) and 2000 points (solid line); (b) centered solutions of (3.1) with $\varepsilon = 0.1$, 0.01, 0.001, and ENO solution for (1.3).

as $\varepsilon \to 0^+$, $0 < A \leqslant \frac{1}{4}$, we plot in Fig. 3c the numerical solutions of (3.1), for $A = \frac{1}{4}$, with $\varepsilon = 0.1$, 0.01, 0.001, and the solution of our scheme for (1.3). The solutions to (3.1) are computed by the standard fourth-order centered scheme with the classical fourth-order Runge–Kutta time discretization. We verify adequate resolution for the solution of (3.1) for each fixed ε by repeatedly refining the mesh until the solutions do not change to visual inspection (the largest number of grid points used is 8000). Clearly we can see the convergence of the solutions of (3.1) to our solution when $\varepsilon \to 0^+$ in Fig. 3c. We remark here that the viscosity–capillarity criterion (3.1) may depend on the capillarity coefficient A [18]. We have not performed extensive numerical study to assess this dependency.

(3) $(v_L, w_L) = (1, 0.45)$, $(v_R, w_R) = (2, 1.5)$. This case is somewhat easier to compute than the previous case, since the initial condition is not a steady nonadmissible weak solution. Figure 4a shows the result with 200 grid points on a solid-line background of a converged solution with 2000 grid points. Figure 4b shows the convergence as $\varepsilon \to 0^+$ of the solutions of the viscosity–capillarity equation (3.1) with $A = \frac{1}{4}$ to our solution.

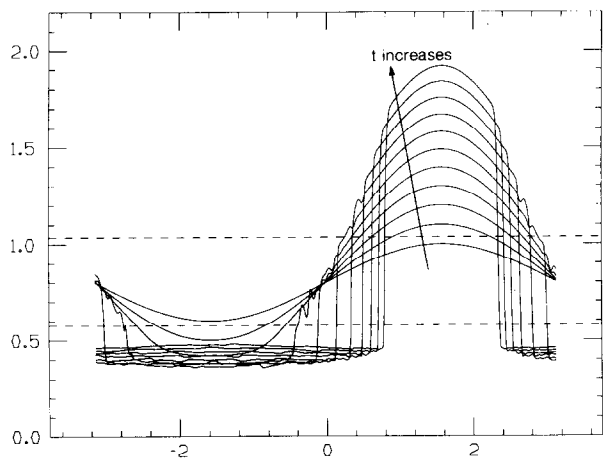

FIG. 5. $(v^0(x), w^0(x)) = (1 - 0.5\cos(x),\ 0.8 + 0.2\sin(x))$. 400 grid points. $t = 0$, 0.2, 0.4, 0.6, 0.8, 1, 1.2, 1.4, 1.6, 1.8, 2.

We then compute the solutions for smooth initial conditions: (1) $(v^0(x), w^0(x)) = (1 - 0.5\cos(x),\ 1 + 0.5\sin(x))$ (it crosses the elliptic regions) and (2) $(v^0(x), w^0(x)) = (1 - 0.5\cos(x),\ 0.8 + 0.2\sin(x))$ (it is contained entirely inside the elliptic region). Periodic boundary condition is used. The solutions gradually evolve into piecewise smooth solutions contained entirely inside one of the two hyperbolic regions $w \leqslant \alpha$ and $w \geqslant \beta$, connected by jumps over the elliptic regions (phase transitions). This seems to agree with the physical intuition. We show the result of (2) in Fig. 5 and omit the graph for (1) which is similar. A numerical vanishing viscosity study (3.1) would be very expensive. Also, for general initial conditions, very little is known about the existence or uniqueness of the limit $\varepsilon \to 0^+$ of (3.1). Notice that during the evolution oscillations are generated inside the elliptic regions (Fig. 5), presumably due to the inherent instability of the equation in those regions. These oscillations fade out once the solution evolves into the hyperbolic regions.

ACKNOWLEDGMENT

I am grateful to Haitao Fan and Din-Yu Hsieh for bringing my attention to the mixed type problems and for many helpful discussions. I also thank the referees for their valuable comments.

REFERENCES

1. J. Bell, J. Trangenstein, and G. Shubin, *SIAM J. Appl. Math.* **46**, 1000 (1986).

2. B. Cockburn, S.-Y. Lin, and C.-W. Shu, *J. Comput. Phys.* **84**, 90 (1989).
3. C. Dafermos, *Arch. Ration. Mech. Anal.* **106**, 243 (1989).
4. H. Fan, *Arch. Rational Mech. Anal.*, to appear.
5. A. Harten, *J. Comput. Phys.* **49**, 357 (1983).
6. A. Harten and S. Osher, *SIAM J. Numer. Anal.* **24**, 279 (1987).
7. A. Harten, B. Engquist, S. Osher, and S. Chakravarthy, *J. Comput. Phys.* **71**, 231 (1987).
8. D.-Y. Hsieh, *J. Math. Phys.* **28**, 1589 (1987).
9. R. D. James, *Arch. Ration. Mech. Anal.* **73**, 125 (1980).
10. B. Keyfitz, *J. Differential Eqs.* **80**, 280 (1989).
11. P. Lax, CBMS Regional Conference Series in Applied Mathematics, Vol. 11 (Conf. Board Math. Sci., Washington, DC, 1973).
12. T.-P. Liu, *J. Differential Eqs.* **18**, 218 (1975).
13. T. Roberts, *J. Comput. Phys.* **90**, 141 (1990).
14. M. Shearer, *Arch. Ration. Mech. Anal.* **93**, 45 (1986).
15. M. Shearer, *Q. Appl. Math.* **46**, 631 (1988).
16. C.-W. Shu and S. Osher, *J. Comput. Phys.* **77**, 439 (1988).
17. C.-W. Shu and S. Osher, *J. Comput. Phys.* **83**, 32 (1989).
18. M. Slemrod, *Arch. Ration. Mech. Anal.* **81**, 301 (1983).
19. M. Slemrod, *Arch. Ration. Mech. Anal.* **105**, 327 (1989).
20. A. Sommerfeld, *Thermodynamics and Statistical Mechanics* (Academic Press, New York/London, 1964).
21. H. Stewart and B. Wendroff, *J. Comput. Phys.* **56**, 363 (1984).
22. G. Strang, *SIAM J. Numer. Anal.* **5**, 506 (1968).
23. B. van Leer, *J. Comput. Phys.* **32**, 101 (1979).

Received July 2, 1990; revised November 30, 1990

CHI-WANG SHU

Division of Applied Mathematics
Brown University
Providence, Rhode Island 02912